Effects of finite laser coherence in quasielastic multiple scattering

T. Bellini, M. A. Glaser, and N. A. Clark
Condensed Matter Laboratory, Department of Physics, University of Colorado, Boulder, Colorado 80309

V. Degiorgio
Dipartimento di Elettronica–Sezione di Fisica Applicata, Università di Pavia, 27100 Pavia, Italy
(Received 1 July 1991)

We have studied the amplitude and temporal correlations of intensity fluctuations of multiply scattered light transmitted through a colloidal suspension. When the coherence length l_c of the incident light becomes comparable to the width of the probability distribution of photon-path lengths, both the amplitude and dynamics of intensity fluctuations become functions of l_c. In this article we present a simple theory that relates these coherence effects to the photon path-length distribution $P(L)$. We have tested this theory using $P(L)$ calculated from computer simulations and from the diffusion approximation, and find that our theory qualitatively accounts for the observed dependences on coherence length. Our results indicate when the effects of finite laser coherence must be taken into account in quasielastic multiple scattering. In the few-scattering regime of quasielastic multiple scattering, we find that the intensity autocorrelation function generally has a stretched-exponential form, and we discuss the origin of this behavior.

PACS number(s): 42.20.−y, 82.70.Dd

I. INTRODUCTION

In diffusing-wave spectroscopy (DWS) [1–3], photons entering a strongly scattering sample are "trapped" in the medium so that, before they can find their way out, they travel distances much larger than the dimensions of the sample [3,4]. Under these conditions, the intensity autocorrelation function $g_2(\tau)$ of the exiting light can be understood on the basis of the time dependence of path lengths in an ensemble of diffusive photon paths. Generally, however, possible corrections to the measured autocorrelation functions due to the finite phase coherence length of the light source are not considered. Such effects should be expected when the *width* of the path-length distribution becomes comparable to the coherence length l_c of the incident light. Maret and Wolf considered these effects in Ref. [5], where they present an expression for the field autocorrelation function for a light source having a finite coherence length, and discuss the effects of finite laser coherence in the backscattering geometry. In this article, we offer a detailed discussion of the effects of the finite coherence length of the light source on both the amplitude and dynamics of the intensity fluctuations of multiply scattered light in the transmission geometry. We have performed light-scattering experiments on a colloidal suspension in an intermediate regime between ordinary quasielastic single scattering (QELS) and DWS. We will refer to this experimental regime, which includes both the few-scattering and diffusive limits of multiple scattering, as quasielastic multiple scattering (QEMS). This choice of experimental conditions allows us to explore the effects of finite phase coherence for experimental conditions ranging from the few-scattering regime to the near-diffusive regime, and to examine the conditions under which the diffusion approximation breaks down.

The ordinary quasielastic single light-scattering technique enables one to measure spectral displacements much smaller than the width of the laser line. This is because the laser fluctuations are essentially phase fluctuations, and because what is measured is not the field autocorrelation function $g_1(\tau)$, but rather the intensity autocorrelation function $g_2(\tau)$. This high resolution remains as long as the scattering volume is smaller than the coherence volume of the incident radiation. In QEMS, the intensity reaching the detector represents the interference between field contributions coming from different paths after varying numbers of scattering events. For strongly scattering media, the exiting radiation can contain contributions from paths whose difference in length is greater than the coherence length l_c of the incident radiation. The interference of such paths fluctuates with a mean period of the order of the coherence time $\tau_c = l_c/c$. For an argon laser without a single moding étalon, such as the one used in the experiments described below, τ_c is about 50 ps, many orders of magnitude smaller than the minimum time resolution of a standard correlator. As a result, the correlation function decays by a significant fraction of its initial value in a time too short to be detected by the correlator. The measured drop in the intensity autocorrelation function is consequently smaller than what would be measured for a perfectly coherent light source. The finite coherence of the light source also affects the dynamics of $g_2(\tau)$, because it decouples contributions to intensity fluctuations from paths having lengths that differ by more than one coherence length.

The article is organized as follows. In Sec. II we describe the experiment and present our experimental results, which demonstrate the effects of finite coherence length on the amplitude and dynamics of intensity fluctuations. In Sec. III we discuss the origin of the observed

effects and derive an expression for $g_2(\tau)$ for a light source having a finite coherence length. The central quantity that enters into this expression for $g_2(\tau)$ is the path-length distribution function $P(L)$. In Sec. IV we calculate the path-length distribution function for the experimental geometry from computer simulations and from the diffusion equation, and compare the results derived from $P(L)$ with the experimental results. The experiment probes a regime intermediate between QELS and DWS, and we show that the diffusion equation does not adequately describe the behavior of multiply scattered light in this regime. In Sec. V we discuss the time dependence of the measured correlation functions and compare these correlation functions with those obtained from computer simulations and from the solution of the diffusion equation. Our results demonstrate that a knowledge of $P(L)$ alone is not sufficient to explain the form of the $g_2(\tau)$ in the few-scattering regime of QEMS. Finally, in Sec. VI we apply our theory to a discussion of the effects of finite coherence length on the dynamical properties of the transmitted light in the diffusive regime.

II. EXPERIMENTAL RESULTS

Because in QEMS the scattering volume is the entire cell, both the position and the direction of the detection line have to be specified. The results described here have been obtained in transmission with a variable distance d between the axis of the incident laser beam and the parallel axis of the detection line. We present experimental results for $g_2(\tau)$ as a function of d and of l_c.

The samples we have used are colloidal suspensions of 0.91-μm-diam polystyrene spheres in water-glycerol mixtures. The scattering mean free path was $l=5.05\pm0.05$ mm in the preparation used here. The cell is large [21.2 $\times$ 46 (horizontal) $\times$ 17mm^3 (vertical)]. The light source is a 514.5-nm argon laser. The beam propagated horizontally and entered the cell at normal incidence at a fixed point on the long lateral side. The incident light was vertically polarized and focused in the center of the cell. The scattered light was collected in the forward direction through a pair of pinholes. The axis defined by the two pinholes was parallel to the incident beam, and its distance d from the axis of the incident beam has been used as an independent variable. We used nine values of d ranging from 3.81 to 25.40 mm. The photon mean free path in this experiment is much longer than the typical values encountered in DWS [1,6,7]. We chose this experimental configuration to enhance the effects of finite laser coherence.

The laser has been used both with and without an intracavity single moding étalon. The full width at half maximum of the laser spectrum in the configuration without the étalon has been measured for various laser intensities using a spectrum analyzer. This yields coherence lengths l_c ranging from 42 (100 mV, minimum power) to 13.5 mm (1400 mV, maximum power). The coherence length for a single mode has been assumed to be longer than 3 m, a value equivalent to $l_c=\infty$ for all the following calculations, being much longer than any other characteristic length in the experiment.

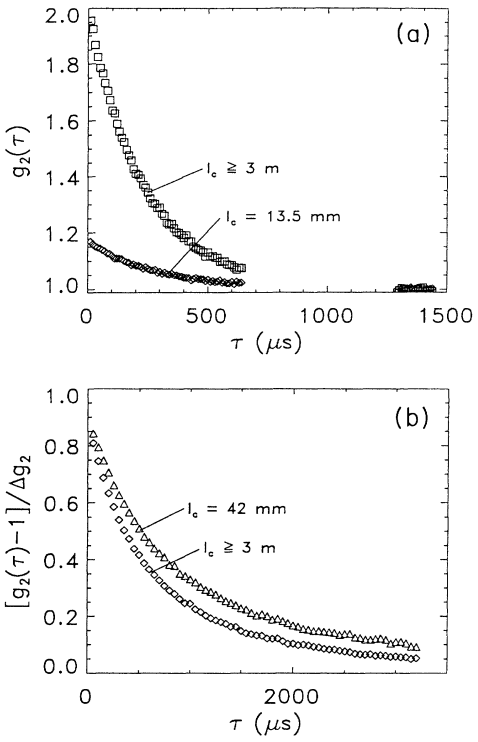

FIG. 1. (a) Experimental intensity autocorrelation functions obtained for $d=25.4$ mm and for small and large l_c. (b) Scaled intensity autocorrelation functions measured for $d=3.81$ mm and for small and large l_c. The time constants are 878 μs ($l_c=42$ mm) and 598 μs ($l_c\geq3$ m).

We found that the overall drop, time constant, and form of the measured correlation functions depend on d and l_c. To obtain an adequate signal, we used a detection system that collects light from a region slightly larger than one coherence area. For all l_c, we have used the measured correlation functions obtained for $l_c=\infty$ to normalize our raw data to one coherence area [8],

$$g_2(\tau;d,l_c)-1 = \left[\frac{g_2^r(\tau;d,l_c)-g_2^r(\tau=\infty;d,l_c)}{g_2^r(\tau=0;d,l_c=\infty)-g_2^r(\tau=\infty;d,l_c=\infty)}\right], \quad (1)$$

where g_2^r is the raw correlation function, and the dependence on d and l_c is indicated explicitly. In Fig. 1(a) we show $g_2(\tau;d,l_c)$ obtained for the largest value of d (25.40 mm) with both short and long coherence lengths. In general, we find that the drop in the correlation function,

$$\Delta g_2(d,l_c)\equiv g_2(\tau=0;d,l_c)-g_2(\tau=\infty;d,l_c) = g_2(\tau=0;d,l_c)-1\ , \quad (2)$$

is equal to 1 for $l_c=\infty$, and is less than 1 for finite l_c. It is important to notice that the $g_2(\tau=0)$ that appears in the preceding formulas is determined by extrapolating $g_2(\tau>0)$ back to $\tau=0$, and so does not contain any decay that occurs in a discontinuous way in the first sample

time of the correlator. As mentioned in the Introduction, the finite coherence length of the laser can lead to a substantial decay of $g_2(\tau)$ in a time too short to be measured by the correlator, so that the measured Δg_2 can be less than 1. The effect of finite coherence length is to reduce the apparent amplitude of intensity fluctuations. In Fig. 1(b), we have compared the *form* of the relaxation for short and long coherence lengths by dividing $g_2(\tau)-1$ by Δg_2, for the smallest d ($d=3.81$ mm). The correlation function obtained with a short coherence length has a slower decay than that obtained with a long coherence length.

The dependence of $\Delta g_2(d,l_c)$ on l_c and d is shown in Figs. 2 and 3. Figure 2 shows $\Delta g_2(d,l_c)$ at $d=5.72$ mm for various l_c obtained by changing the intensity of the laser. In Fig. 3 we present $\Delta g_2(d,l_c)$ measured for various d with two different laser intensities. Figures 2 and 3 demonstrate that the amplitude of intensity fluctuations decreases with decreasing l_c or increasing d.

The correlation functions are nearly exponential only for the largest two values of d. For smaller d, the correlation functions obtained both with and without the étalon are not exponential and can be well fitted by the stretched-exponential form $g_2(\tau)\propto\exp[-(\tau/\tau_s)^{\alpha}]$. The exponent α and time constant τ_s are functions of d. In Fig. 4 we show stretched-exponential fits of $g_2(\tau;d,l_c=\infty)$ for three different values of d. This figure illustrates that α is a function of d. In Table I we present the values of α obtained for various d, both with and without the étalon (rows 3 and 4, respectively). The values of α obtained with a small coherence length are systematically larger than those obtained with large l_c, although the effect is small. The fact that we in general observe strongly nonexponential relaxation indicates that our experiment has been performed in the few-scattering regime of QEMS, because the decay of the transmitted intensity autocorrelation function is expected to be nearly exponential in the diffusive regime [3].

To study the dependence of the decay time on d and l_c, we used the time constant $T(d,l_c)$, defined as follows:

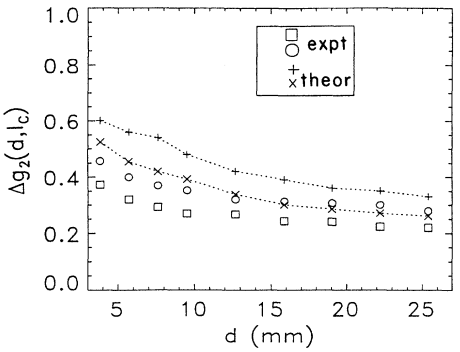

FIG. 3. Overall drop of the intensity autocorrelation function $\Delta g_2(d,l_c)$ as a function of d for fixed l_c: (□) $l_c=13.5$ mm, experiment; (○) $l_c=18.0$ mm, experiment; (×) $l_c=13.5$ mm, calculated; (+) $l_c=18.0$ mm, calculated.

$$T(d,l_c)=\frac{1}{\Delta g_2(d,l_c)}\int_0^{\infty}d\tau[g_2(\tau;d,l_c)-1]\ . \tag{3}$$

$T(d,l_c)$ is one of the equivalent definitions of time constant for exponential decays. In the case of stretched exponentials, this quantity is less sensitive to the initial part of the decay than is τ_s. In Fig. 5, we show the dependence of $T(d,l_c)$ on d for both small and large coherence lengths. Notice that the experiment done with the shorter coherence length gives systematically slower decays.

III. THEORY

Because the laser fluctuations are phase fluctuations, the incident field can be written

$$E_{\rm inc}(t)=E_c(t)\exp[i\Phi(t)]\ ,$$

where $E_c(t)$ is a perfectly coherent field and $\exp[i\Phi(t)]$ contains the phase fluctuations. For simplicity, we consider the electric field of the scattered light to be a scalar field, as in Ref. [2]. The field reaching the detector can be

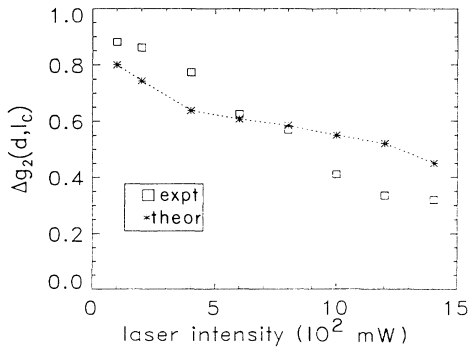

FIG. 2. Overall drop of the intensity autocorrelation function $\Delta g_2(d,l_c)$ as a function of laser intensity without the étalon for $d=5.72$ mm, showing the decrease of $\Delta g_2(d,l_c)$ with decreasing l_c: (□) experimental results; (*) theoretical calculation.

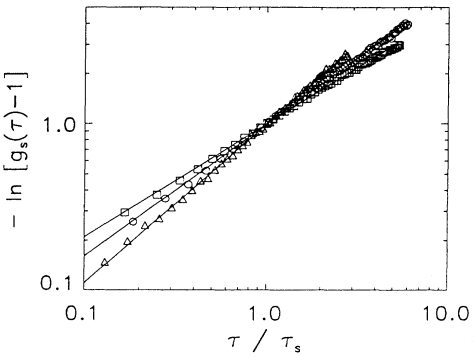

FIG. 4. Intensity autocorrelation functions obtained in the configuration with the étalon for three different values of d: $d=3.81$ mm (squares), $d=9.53$ mm (circles), and $d=25.4$ mm (triangles). The straight line is the stretched-exponential fit and the slope is equal to the exponent α.

written as a sum of contributions from groups of paths of nearly the same length, where the path difference between adjacent "channels" is much smaller than l_c. The field reaching the detector is therefore

$$E(t)=\sum_j E_{jc}(t)\exp[i\Phi_j(t)]\ , \tag{4}$$

where $E_{jc}(t)$ is the field scattered through the paths of length L_j when the input field is totally coherent and

$$\langle \exp[i\Phi_j(t)]\exp[-i\Phi_k(t+\tau)]\rangle = \exp\{-[(L_k-L_j+c\tau)/l_c]^2\}\ . \tag{5}$$

A Gaussian shape for the laser spectrum has been assumed (appropriate for the argon laser used in the experiment). When the spectrum of the source is predominantly Lorentzian, Eq. (5) becomes

$$\langle \exp[i\Phi_j(t)]\exp[-i\Phi_k(t+\tau)]\rangle = \exp\{-[(L_k-L_j+c\tau)/l_c]\}\ . \tag{6}$$

The time required for the light to traverse the longest paths is too short to be detected by the correlator and is much shorter than the characteristic time of the system dynamics. When $\tau \gg |L_j-L_k|/c$ for every k and j and $\tau \gg cl_c$ [9], we find

$$\begin{aligned} g_2(\tau)&=\frac{\langle I(t)I(t+\tau)\rangle}{\langle I(t)\rangle^2} \\ &=\frac{1}{\langle I(t)\rangle^2}\sum_{j,k,l,m}\langle E_{jc}(t)E^*_{kc}(t)E_{lc}(t+\tau)E^*_{mc}(t+\tau)\rangle \\ &\quad\times\langle \exp[i\Phi_j(t)]\exp[-i\Phi_k(t)]\exp[i\Phi_l(t+\tau)]\exp[-i\Phi_m(t+\tau)]\rangle \\ &=\frac{1}{\langle I(t)\rangle^2}\left[\sum_{j,l}\langle I_j(t)I_l(t+\tau)\rangle+\sum_{j,k}\langle I_j(t)\rangle\langle I_k(t)\rangle g_{1j}(\tau)g_{1k}(\tau)e^{-2[(L_k-L_j+c\tau)/l_c]^2}\right] \\ &=1+\int_0^\infty dL\int_0^\infty dL'P(L)P(L')g_1(L,\tau)g_1(L',\tau)e^{-2[(L-L')/l_c]^2}\ , \end{aligned} \tag{7}$$

where $g_{1j}(\tau)=\langle E_{jc}(t)E^*_{jc}(t+\tau)\rangle/\langle I_j(t)\rangle$. This equation is similar to the one proposed in Ref. [5], although it has been deduced for the intensity autocorrelation function rather than the field autocorrelation function. Also, Eq. (7) shows that the identification of $g_2(\tau)$ with $g_1^2(\tau)+1$ is appropriate only when the coherence length is infinite, so that Eq. (14) in Ref. [5] is not strictly correct as it stands. When $P(L)=\delta(L-L_0)$ (where δ is the Dirac delta func-

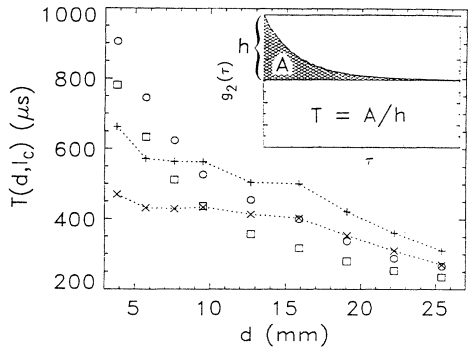

FIG. 5. Time constant $T(d,l_c)$ as a function of d for fixed laser intensity, both with and without the étalon: (□) $l_c \geq 3$ m, experimental; (○) $l_c=13.5$ mm, experimental; (×) $l_c=3$ m, calculated; (+) $l_c=13.5$ mm, calculated. The graphical definition of $T(d,l_c)$ is shown in the inset.

TABLE I. Exponents α obtained from stretched-exponential fits to the intensity autocorrelation functions. Each column refers to fixed position d of the detector. $\langle n\rangle$ is the average number of scattering events (from the simulation). The first two rows list α obtained by fitting the experimental correlation functions in the configurations with and without the étalon ($l_c=\infty$ and 18 mm, respectively). The last five rows list the results for the correlation functions calculated from the computer simulation (S) and from the diffusion equation (D), using Eq. (12) [$P(Q^2)$] or Eqs. (7) and (9) [$P(L)$].

d	3.81	5.72	7.62	9.53	12.70	15.88	19.05	22.23	25.40
$\langle n\rangle$	5.77	6.63	7.18	7.74	9.11	10.14	11.00	11.56	12.59
E: $l_c=\infty$	0.68	0.70	0.75	0.76	0.80	0.84	0.90	0.92	0.92
E: $l_c=18$ mm	0.75	0.77	0.79	0.81	0.87	0.91	0.96	0.98	0.98
S: $P(Q^2)$, $l_c=\infty$	0.68	0.70	0.73	0.77	0.78	0.82	0.85	0.86	0.89
S: $P(L)$, $l_c=\infty$	0.98	0.97	0.97	0.97	0.97	0.97	0.97	0.97	0.97
S: $P(L)$, $l_c=18$ mm	0.98	0.98	0.98	0.98	0.98	0.98	0.98	0.98	0.99
D: $P(L)$, $l_c=\infty$	0.93	0.93	0.93	0.93	0.93	0.94	0.94	0.95	0.95
D: $P(L)$, $l_c=18$ mm	0.94	0.94	0.94	0.94	0.95	0.95	0.95	0.95	0.96

tion) Eq. (7) reduces to the ordinary relation between $g_2(\tau)$ and $g_1(\tau)$ in QELS.

From Eq. (7), it is easily seen that the drop in the intensity autocorrelation is given by

$$\Delta g_2 = \int_0^\infty dL \int_0^\infty dL' P(L) P(L') e^{-2[(L-L')/l_c]^2} . \quad (8)$$

Because $P(L)$ is normalized, Eq. (8) shows that Δg_2 is always less than or equal to 1.

From Eq. (7) it follows that the shape of $g_2(\tau)$ also is affected by the value of l_c. We assume a τ dependence for $g_1(L,\tau)$ that has already been consistently assumed for strongly scattering media [1,2], namely

$$g_1(L,\tau) = \exp(-\gamma L \tau) . \quad (9)$$

$\gamma = D_s \langle q^2 \rangle / l$, where D_s is the self-diffusion constant of scatterers, l is the photon mean free path, and $\langle q^2 \rangle$ is the average of the square of the scattering vector performed according to the differential cross section of the scatterers. With this assumption we can obtain the time constant of intensity fluctuations from Eqs. (3) and (7):

$$T = \frac{1}{\Delta g_2} \int_0^\infty dL \int_0^\infty dL' \frac{P(L) P(L') e^{-2[(L-L')/l_c]^2}}{\gamma (L + L')} . \quad (10)$$

Equation (9) is really only appropriate in the diffusive regime of QEMS. As discussed in more detail in Sec. V, Eq. (9) gives a poor description of the behavior of $g_1(L,\tau)$ in the few-scattering regime. As a result, Eq. (10) has only approximate validity in the few-scattering regime.

If we knew the path-length distribution $P(L;d)$ for the experimental situation discussed in Sec. II, we could calculate $\Delta g_2(d,l_c)$ and $T(d,l_c)$ for various l_c from Eqs. (8) and (10). The foregoing analysis implies that, to the degree of approximation implicit in Eq. (9), the dependence of both $\Delta g_2(d,l_c)$ and $T(d,l_c)$ on d derives entirely from the d-dependence of $P(L;d)$. In the following section we describe two methods for calculating $P(L;d)$ for the experimental configuration and compare $\Delta g_2(d,l_c)$ and $T(d,l_c)$ calculated from $P(L;d)$ with the experimental results.

IV. CALCULATION OF THE PATH-LENGTH DISTRIBUTION

To test the theory directly, we have calculated $P(L;d)$ in two different ways: (i) from a computer simulation that traces photons whose mean free path and differential cross section were chosen to match the experimental situation as closely as possible, and (ii) by solving the appropriate diffusion equation. In both cases the dimensions of the sample cell and the detector positions matched those in the experiment.

To obtain reasonably good statistics in the simulation, photons were collected from much larger areas of the front cell surface and for a much wider range of exit angles than in the experiment. Each photon trajectory was a weighted random walk, with step sizes chosen from an exponential distribution having a decay constant equal to the scattering photon mean free path l, and scattering angles chosen from a Lorentzian differential cross section with a width chosen to give the correct ratio of forward to back scattering for the colloidal particles and solvent used in the experiment. For simplicity, we neglected the dependence of the differential cross section on photon polarization. Each photon trajectory was traced until the photon emerged from the cell, and a contribution was added to the $P(L;d)$ distribution if the photon emerged within one of the output channels. 10^9 photons were traced, of which $\sim 2\times 10^5$ emerged in the nine output channels. Figure 6 shows five simulated photon trajectories that emerge in the output channel at $d = 15.88$ mm. The $P(L;d)$ distributions obtained from the simulations for several values of d are shown in Fig. 7(a). As d increases, the $P(L;d)$ distributions broaden and the mean values and most probable values of L both increase.

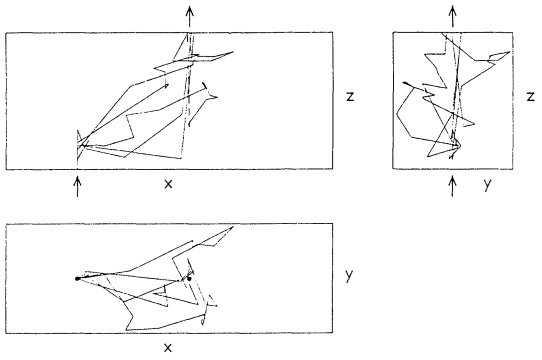

FIG. 6. Typical photon trajectories from the computer simulation, projected onto the three orthogonal planes. The x-z plane is the horizontal plane, and the incident photons are initially propagating in the z direction. We have shown five trajectories that emerge in the output channel at $d = 15.88$ mm.

In the simulation we have also obtained the distribution of scattering events $P(n;d)$, where n is the number of scattering events for a given photon path. The $P(n;d)$ distributions for several values of d are shown in Fig. 7(b). These distributions clearly show that we are in a regime intermediate between QELS and DWS. The mean number of scattering events $\langle n \rangle$, as a function of d, is shown in the second row of Table I. $\langle n \rangle$ ranges from 5.77 for $d = 3.81$ mm to 12.59 for $d = 25.40$ mm. We have also obtained the distribution of $Q^2 = \sum_i q_i^2$, $P(Q^2;d)$, where the sum runs over scattering events for a single photon path and q_i^2 is the squared scattering vector for the ith scattering event. This distribution is used in Sec. V to explain the shape of the intensity autocorrelation function. The $P(Q^2;d)$ distributions for several values of d are shown in Fig. 7(c). The distinct peak in $P(Q^2;d = 3.81$ mm) near $Q^2 = 0$ appears to be the result of two-scattering processes.

The diffusion equation for light in highly turbid media [see Eqs. (16) and (17) in Ref. [3]] has been solved for a point source placed at the spot where the laser enters the sample. The solution is similar to the one described in

Sec. V [see Eqs. (13) and (14)] for a geometry of more general interest. In Figs. 8(a) and 8(b) we compare the $P(L;d)$ obtained from the diffusion calculation with those from the simulation for $d=3.81$ and 25.40 mm, respectively. For $d=3.81$ mm, the agreement between the two distributions is poor. In particular, the small-L part of $P(L;d)$ obtained from the diffusion equation is unphysical, as it gives a finite probability for path lengths shorter than the distance between the incoming and outgoing spots. For increasing d the unphysical small-L part of $P(L;d)$ is still present in the solution of the diffusion equation, but the overall agreement between the two distributions improves. This suggests that our experiment is in the near-diffusive regime only for the largest values of d. For this reason, only the simulation results have been compared with the experimental results.

From the $P(L;d)$ obtained from the simulation, we calculated $\Delta g_2(d;l_c)$ and $T(d,l_c)$ as a function of d for various values of l_c, using Eqs. (8) and (10). Notice that in all the calculations there are no adjustable parameters: l_c and γ, the mean free path and the scattering cross section, have all been measured or deduced from the experiment. In Figs. 2 and 3, we present the values of $\Delta g_2(d,l_c)$ calculated from the simulation using Eq. (8) and in Fig. 5 we display the values obtained for $T(d,l_c)$ via Eq. (10). We obtain good qualitative agreement with the experimental results. This demonstrates the adequacy of our theoretical description in explaining the observed effects.

The agreement with the experimental results could perhaps be improved by enhancing the statistics of the $P(L)$ distributions and by including the effects of photon polarization in the differential cross section. It is also worth reiterating that the assumed functional form of $g_1(L,t)$ [Eq. (9)] that leads to Eq. (10) is correct only for photon paths with many scattering events, while the mean number of scatterings, as given by the simulation, is not large ($5.77 \leq \langle n \rangle \leq 12.59$). We will discuss the validity of this approximation in more detail in the following section.

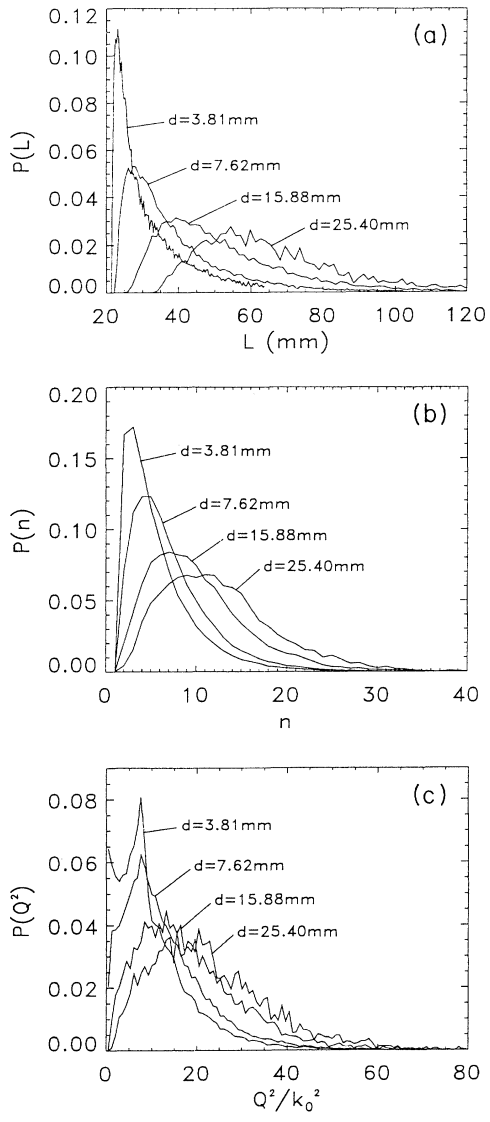

FIG. 7. Distributions obtained from the computer simulation for several values of d: (a) photon path-length distribution $P(L;d)$; (b) distribution of the number of scattering events per path $P(n;d)$; (c) distribution of Q^2 per path $P(Q^2;d)$.

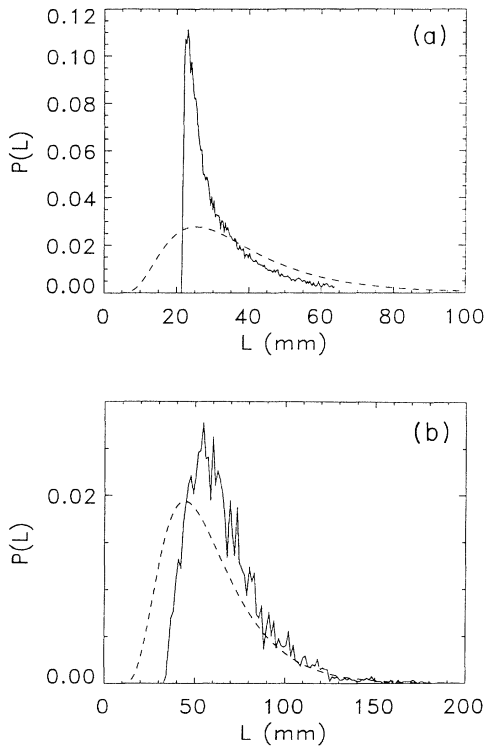

FIG. 8. Comparison between $P(L;d)$ obtained from simulation (solid line) and from the diffusion approximation (dashed line): (a) $d=3.81$ mm; (b) $d=25.4$ mm.

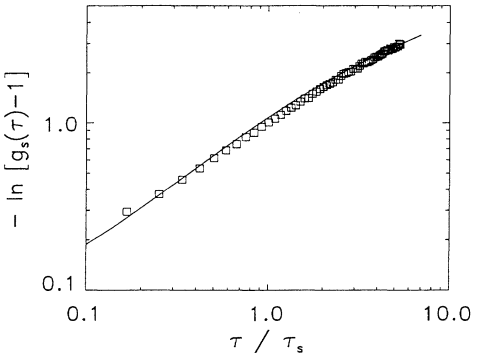

FIG. 9. Intensity autocorrelation functions for $d=3.81$ mm measured in the configuration with étalon (□) and calculated from $P(Q^2;d)$ obtained from the simulation (solid line). For both the curves the stretched-exponential fit gives $\alpha=0.68$.

V. FORM OF THE INTENSITY AUTOCORRELATION FUNCTION

As mentioned above, the intensity autocorrelation functions obtained in the experiment generally have a stretched-exponential form. The results presented in the third and fourth rows of Table I show that the relaxations are less exponential when $\langle n \rangle$ is small and that the effect of finite coherence length on α is small. We have found that the information contained in $P(L;d)$ is not sufficient to explain the shape of the experimental decays. As shown in rows 6–9 in Table I, the exponent α obtained by fitting the $g_2(\tau;d,l_c)$ calculated from $P(L;d)$ via Eqs. (7) and (9) is approximately 1 independent of d and l_c, for both the simulation and the diffusion approximation. An understanding of the stretched-exponential decay in this regime requires the knowledge of $P(Q^2;d)$. In the limit $l_c \to \infty$, the field autocorrelation function can be calculated from $P(Q^2;d)$ from

$$g_1(\tau) \propto \sum_{\text{paths}} e^{-Q^2 D_s t} , \tag{11}$$

which can be rewritten

$$g_1(\tau) = \int dQ^2 P(Q^2) e^{-Q^2 D_s t} . \tag{12}$$

In this limit $g_2(\tau)=g_1^2(\tau)+1$. The values of α obtained from Eq. (12) using the $P(Q^2;d)$ distributions from the simulation are shown in the fifth row of Table I, and are observed to have the same dependence on d as the experimental results for $l_c=\infty$, when fitted with a stretched exponential in the experimental time interval. The values of α obtained from $P(Q^2;d)$ are nearly the same as those obtained from $P(L;d)$ for the two largest values of d. In Fig. 9 we have shown the intensity autocorrelation function obtained from the simulation using $P(Q^2;d)$ for $d=3.81$ mm, together with the one experimentally measured. The calculated correlation decay exhibits a slight curvature not present in the experimental data, which indicates that even this approach has some intrinsic limitations, perhaps due to the neglect of photon polarization in the simulation. Overall, the results of Table I demonstrate that when the average number of scattering events $\langle n \rangle$ is small (<10), Q^2 cannot be approximated by $L\langle q^2 \rangle / l$ and, therefore, $P(Q^2;d)$ and $P(L;d)$ are independent. This can be seen by comparing Figs. 7(a) and 7(c). The width of $P(L;d)$ increases dramatically with increasing d, while the width of $P(Q^2;d)$ is nearly independent of d.

To gain a better understanding of the origin of the shape of the decay of the intensity autocorrelation function in transmission, we have solved the diffusion equation for a point source on the face of a slab of thickness L_s and of infinite lateral extention. We have obtained the path-length distribution in transmission as a function of the radial offset ρ, which is

$$P(L,\rho) \propto \left[\sum C_m \exp\left[-\frac{\lambda_m^2 \beta L}{2} \right] \right] \times \left[\frac{1}{2\pi\beta L} \exp\left[-\frac{\rho^2}{2\beta L} \right] \right] , \tag{13}$$

where

$$C_m = \frac{4\lambda_m^2 \beta [\sin(\lambda_m L_s) + \lambda_m \beta \cos(\lambda_m L_s)]}{2\lambda_m L_s(\lambda_m^2\beta^2+1) + 4\lambda_m \beta \sin^2(\lambda_m L_s) + (\lambda_m^2\beta^2-1)\sin(2\lambda_m L_s)}$$

and the λ_m are the solutions of

$$\tan(\lambda L_s) = \frac{2\lambda\beta}{\lambda^2\beta^2-1} . \tag{14}$$

Here $\beta - \frac{2}{3} l^*$ and l^* is the transport mean free path, defined in terms of the scattering mean free path l as $l^* = 2lk_0^2/\langle q^2 \rangle$, where k_0 is the wave vector of the incident light. For $l^*/L_s \leq 0.2$, $P(L;\rho=0)$ is well approximated by the equation

$$P(L,\rho=0) = \frac{A}{L} \exp\left[-\frac{\zeta L_s^2}{2\beta L} \right] \times \left[\exp\left[-\frac{\lambda_a^2 \beta L}{2} \right] + B \exp\left[-\frac{\lambda_b^2 \beta L}{2} \right] \right] , \tag{15}$$

where ζ is a number close to 1, λ_a is close to the lowest-

order solution of Eq. (14), and λ_b and B are fitting parameters that take into account the effect of higher-order terms [the case $\rho>0$ can be treated by replacing L_s^2 by $L_s^2+\rho^2$ in Eq. (15)]. A fit of $P(L,\rho=0)$ to Eq. (15) for $l^*/l_s=0.01$ is shown in Fig. 10. The intensity autocorrelation function calculated from Eqs. (7), (9), and (15) is, in the limit $l_c\to\infty$,

$$g_2(\tau)\propto\left\{K_0\left[\xi^{1/2}\left[\lambda_a^2L_s^2+\frac{8k_0^2L_s^2}{3\beta^2}D_s\tau\right]^{1/2}\right]+BK_0\left[\xi^{1/2}\left[\lambda_b^2L_s^2+\frac{8k_0^2L_s^2}{3\beta^2}D_s\tau\right]^{1/2}\right]\right\}, \quad (16)$$

where K_0 is a zeroth-order modified Bessel function. This correlation function exhibits a crossover from exponential behavior at small τ to a stretched-exponential form with $\alpha=\frac{1}{2}$ for long times. Neglecting power-law corrections, $g_2(\tau)\simeq\exp[-(E+F\tau)^{1/2}]$, where $E\approx4\lambda_b^2L_s^2$ and $F\approx32k_0^2L_s^2D_s/(3\beta^2)$. For small τ, $(E+F\tau)^{1/2}\approx E^{1/2}[1+(F/2E)\tau]$, so that the time constant for the intial exponential decay is $\tau_e\approx2E^{1/2}/F$. The crossover time τ_x after which $g_2(\tau)$ has a stretched-exponential form with $\alpha=\frac{1}{2}$ to a good approximation is determined by solving the equation $(E+F\tau_x)^{1/2}=(F\tau_x)^{1/2}(1+\epsilon)$, where ϵ is a small number. With $\epsilon=0.1$ we find that $\tau_x/\tau_e=E^{1/2}/(4\epsilon)=\lambda_bL_s/(2\epsilon)\approx30$ for $l^*/L_s\leq0.2$. This estimate explains why the asymptotic stretched-exponential behavior of $g_2(\tau)$ is difficult to observe experimentally. In fact, the correlation function calculated form Eq. (16) is nearly exponential in the restricted interval $0<\tau<4\tau_e$ (an exponent of $\alpha=0.89$ is obtained from a stretched-exponential fit in this time interval for $l^*/L_s=0.01$).

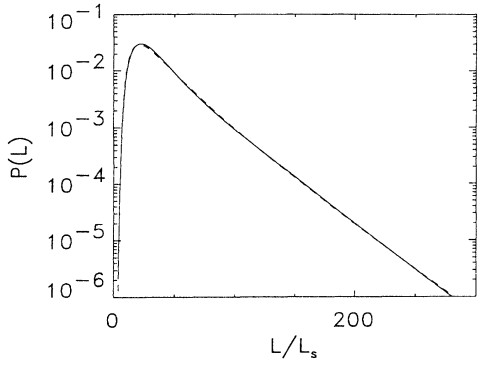

FIG. 10. $P(L,\rho=0)$ calculated from Eq. (13) for $l^*/L_s=0.01$ (solid line), together with a fit to Eq. (15) (dashed line). The fitting parameters are $\xi=0.81$, $\lambda_a=1.03\lambda_1$, and $\lambda_b=0.84\lambda_2$. λ_1 and λ_2 are the first two solutions of Eq. (14). The fitting parameters in the case $l^*/L_s=0.05$ are $\xi=0.85$, $\lambda_a=1.03\lambda_1$, and $\lambda_b=0.82\lambda_2$.

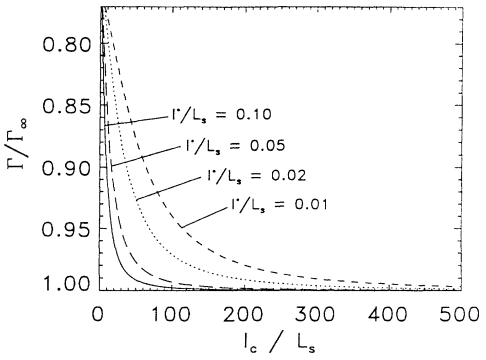

FIG. 11. First cumulant Γ of the intensity autocorrelation function calculated from Eq. (17) as a function of l_c/L_s for various l^*/L_s. The four curves have been rescaled with the value of Γ obtained when $l_c/L_s\to\infty$, given here in units of $D_sk_0^2$: $l^*/L_s=0.01$, $\Gamma_\infty=1.44\times10^4$; $l^*/L_s=0.02$, $\Gamma_\infty=3.75\times10^3$; $l^*/L_s=0.05$, $\Gamma_\infty=6.42\times10^2$; $l^*/L_s=0.10$, $\Gamma_\infty=1.77\times10^2$.

VI. EFFECTS OF FINITE COHERENCE LENGTH IN THE DIFFUSIVE REGIME

In the preceding section, we described the solution of the diffusion equation for an infinite slab. In this section, we use this solution to investigate the effects of finite coherence length in the diffusive regime, for the particular case $\rho=0$ (the case $\rho>0$ is expected to exhibit qualitatively similar behavior). In Fig. 11 we show the l_c dependence of the first cumulant of the transmitted intensity autocorrelation function Γ for several values of l^*/L_s. In Fig. 12 we show the analogous plot for the time constant T. Γ has been calculated from its definition [10] and Eqs. (7)–(9):

$$\Gamma=-\frac{2D_sk_0^2}{\Delta g_2}\int dL\int dL'P(L)P(L')\left[\frac{L+L'}{l^*}\right]\times e^{-2[(L-L')/l_c]^2}, \quad (17)$$

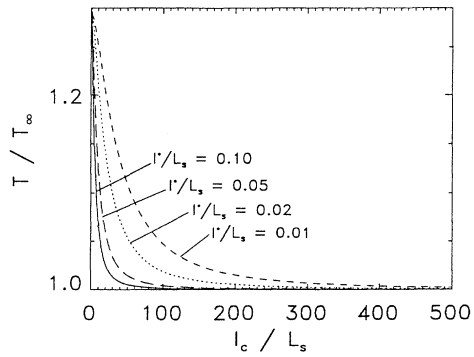

FIG. 12. Time constant T of the intensity autocorrelation function calculated from Eq. (10) as a function of l_c/L_s for various l^*/L_s. The four curves have been rescaled with the value of T obtained when $l_c/L_s\to\infty$, given here in units of $1/(D_sk_0^2)$: $l^*/L_s=0.01$, $T_\infty=8.17\times10^{-5}$; $l^*/L_s=0.02$, $T_\infty=3.17\times10^{-4}$; $l^*/L_s=0.05$, $T_\infty=1.86\times10^{-3}$; $l^*/L_s=0.10$, $T_\infty=6.78\times10^{-3}$.

and Eq. (10) has been used to calculate T. Figures 10 and 11 support our previous conclusion that the decay of the intensity autocorrelation function becomes slower as the coherence length decreases. Our results demonstrate that finite coherence length significantly affects both Γ [which is sensitive to the short-time behavior of $g_2(\tau)$] and T (which reflects the intermediate-time behavior). Our result for transmission differs somewhat from that obtained by Maret and Wolf in backscattering, where the effect of finite coherence length is more noticeable in the short-time behavior of $g_2(\tau)$ (see Fig. 6 of Ref. [5]). This can be understood from Eq. (17), which also holds in the backscattering geometry, the only difference being in $P(L)$. Adopting for $P(L)$ the approximate expression for backscattering, $P(L) \propto L^{-3/2} e^{W/L}$ [5], where W is a constant, it is easily shown that a finite coherence length suppresses the divergence of Γ. This drastic change in the shape of $g_2(\tau)$ induced by the finiteness of l_c is a consequence of the power-law decay of $P(L)$ for large L.

ACKNOWLEDGMENTS

We thank Mr. Art Klittnick for his valuable technical assistance. One of us (T.B) acknowledges support from NATO. This work was supported by NSF Grant No. DMR-8807443, and was partially supported by the National Center for Supercomputing Applications under Grant No. DMR-900011N.

[1] D. J. Pine, D. A. Weitz, P. M. Chaikin, and E. Herbolzheimer, Phys. Rev. Lett. **60**, 1134 (1988).

[2] F. C. MacKintosh and S. John, Phys. Rev. B **40**, 2383 (1989).

[3] D. J. Pine, D. A. Weitz, G. Maret, P. E. Wolf, E. Herbolzheimer, and P. M. Chaikin, in *Scattering and Localization of Classical Waves in Random Media,* edited by P. Sheng (World Scientific, Singapore, 1990).

[4] G. H. Watson, Jr., P. A. Fleury, and S. L. McCall, Phys. Rev. Lett. **58**, 945 (1987).

[5] G. Maret and P. E. Wolf, in *Scattering in Volumes and Surfaces,* edited by M. Nieto-Vesperians and J. C. Dainty (North-Holland, Amsterdam, 1990).

[6] I. Freund, M. Kaveh, and M. Rosenbluh, Phys. Rev. Lett. **60**, 1130 (1988).

[7] S. Fraden and G. Maret, Phys. Rev. Lett. **65**, 512 (1990).

[8] N. C. Ford, Jr., in *Dynamic Light Scattering,* edited by R. Pecora (Plenum, New York, 1985).

[9] P. Pusey, in *Correlation and Light Beating Spectoscopy,* edited by H. Z. Cummins and E. R. Pike (Plenum, New York, 1974).

[10] B. J. Berne and R. Pecora, *Dynamic Light Scattering* (Wiley, New York, 1985).